Evaluation of the TiO_2 Anti-Reflective Coating in PERT Solar Cells with Silicon Dioxide Passivation

Izete Zanesco, Adriano Moehlecke, José C. M. Model, Moussa Ly, Jéssica de Aquino, Ricardo Augusto Zanotto Razera, Thais Crestani, Vanessa da Conceição Osório and Vanessa Alves Gonçalves

Solar Energy Technology Nucleus, School of Technology, Pontifical Catholic University of Rio Grande do Sul – PUCRS, Porto Alegre (Brazil)

Abstract

The PERC solar cell family is manufactured by the industry because the passivation of both faces can improve the efficiency. The passivation and anti-reflective (AR) coating is usually performed using silicon nitride. However, the silicon dioxide may produce a good passivation in the emitter and in the boron BSF. The goal of this paper is to present the analysis of the TiO_2 AR coating in PERT solar cells passivated with SiO_2. Based on previous studies, the dry oxidation was performed at 800 °C and 860 °C, growing the SiO_2 layer on the phosphorus emitter of 50 nm and 60 nm, respectively. The thickness of the TiO_2 AR coating evaporated by e-beam technique was optimized and the SiO_2/TiO_2 double layer was analyzed by the comparison of the electrical parameters and internal quantum efficiency of the PERT solar cells and the reflectance of the double layer. The efficiency of 16.8 % was achieved with 37 nm TiO_2 coating and SiO_2 layer grown at 800 ºC. The firing of the conductive pastes reduced the thickness of the SiO_2/TiO_2 layer and the lowest weighted average reflectance was 2.8 %. The solar cells with thinner TiO_2 coat presented low internal quantum efficiency in wavelengths higher than 700 nm.

Key-words: silicon solar cells, titanium dioxide anti-reflective coating, silicon dioxide passivation.

1. Introduction

In the last decade, the industrial process to manufacture silicon solar cells was based on the aluminum back surface field (Al-BSF), formed with conductive paste screen-printed on the rear face of p-type silicon wafers and fired in a belt furnace. During the firing process, the solar cells bowed and the devices could break during the module assembling. Moreover, the passivation of the full area Al-BSF is limited. Nowadays, the PERC (passivated emitter and rear cell) structures, such as PERT (passivated emitter, rear totally-diffused), PERL (passivated emitter, rear locally-doped), PERD (passivated emitter, rear directly-contacted) and PERF (passivated emitter, rear floating-junction) cells, are gaining the market share, dominated by the aluminum back surface field technology (Colville, 2017; Green, 2015; ITRPV, 2019). The main advantages of PERC structure with boron back surface field (B-BSF) are 1) to avoid the bowing of the monocrystalline Czochralski silicon (Cz-Si) wafers and the multicrystalline silicon wafers and 2) to allow the passivation of the BSF surface, besides of the front emitter, that reduces the minority charge carrier recombination and improves the internal reflectance of the rear face. This structure of solar cell presents one of the best potential to achieve high efficiency and, consequently, to manufacture photovoltaic modules at competitive prices. The PERT cell is one structure of the PERC family and can be manufactured with a cost-effective process. In this paper, the TiO_2 anti-reflective coating of the PERT cell with boron BSF and SiO_2 passivation was evaluated.

The industry has been manufactured silicon solar cells with silicon nitride as anti-reflective (AR) coating and passivation layer, deposited on the phosphorus emitter by plasma-enhanced chemical vapor (PECVD) method. This material provides low surface recombination velocity because the presence of positive interface charges,

Selection and/or peer review under responsibility of Scientific Committee
doi:10.18086/swc.2019.19.13 Available at http://proceedings.ises.org

that produces a field effect passivation (Lelièvre et al., 2019; Liu et al., 2018; Rahman and Khan, 2012). Nevertheless, the thermally grown SiO_2 is the most effective dielectric layer to passivate the n^+ emitter as well as the boron doped back surface field (Glunz and Feldmann, 2018). A SiO_2 layer of only 10 nm is enough to passivate the phosphorus emitter (Zanesco and Moehlecke, 2015). The SiO_2 layer can be simultaneously grown in both faces of the silicon wafer by dry oxidation. However, silicon dioxide has a low refractive index and, consequently, it is not a good material to form the AR coating. Then, the silicon dioxide is usually combined with other materials to reduce the reflectance (Chen et al., 2017; Huang et al., 2018; Preissler et al., 2018). On the other hand, titanium dioxide may not provide effective surface passivation, but this material is used to form the AR coating because presents low absorption at short wavelengths and has a high refractive index. The passivation with titanium dioxide depends on the technique used to deposit the layer and new methods have been developed. For instance, the chemical ultrasonic spray deposition was used to produce a single layer of TiO_2 and the reflectance of textured silicon wafers was 5 % (Sali et al., 2017). The spin coating procedure was applied to deposit a TiO_2/SiO_2 thin film. Solar cells with the TiO_2/SiO_2 stack coating achieved the efficiency of 18.2 % (Lee et al., 2015). Using the sputtering technique, a TiO_2/SiO_2 stack layer was deposited on non-textured surface of p-type silicon wafers and the average reflectance was 7 % (Ali et al., 2014). The TiO_2 film was also combined with Al_2O_3 (Suh, 2019). This double layer was formed by low cost spray pyrolysis on silicon solar cells. The average efficiency obtained was 15.5% (Kanda et al., 2016).

Bearing in mind the need to passivate both faces of the PERC solar cells, the effective passivation provided by silicon dioxide in n^+ and p^+ heavily doped regions, the growth of the SiO_2 in both faces during the dry oxidation process and the features of titanium dioxide like the AR coating material, the goal of this paper is to present the evaluation of the TiO_2 AR coating deposited over the SiO_2 passivation layer on the front phosphorus emitter of PERT solar cells by the analysis of the electrical parameters and internal quantum efficiency of the solar cells and the reflectance of the TiO_2/SiO_2 double layer. Based on previous studies (Zanesco et al., 2018[a]), the dry oxidation was performed with two temperatures and, for each SiO_2 thickness, the TiO_2 AR coating deposited by electron beam evaporation technique (e-beam) was experimentally optimized.

2. Silicon solar cells process and development of the anti-reflective coating

The Fig. 1 presents the structure of the PERT solar cell developed using solar grade p-type Cz-Si wafers with thickness of 200 µm and base resistivity from 1 Ω.cm to 20 Ω.cm. The process sequence was optimized in a previous work (Zanesco et al. 2018[b]) and is summarized in the following steps: texture etching, RCA wet-chemical cleaning, deposition of the liquid with boron by spin coating technique, boron diffusion and oxidation in a quartz tube furnace, oxide etching in the front face and RCA chemical cleaning, phosphorus diffusion, boron and phosphorus silicate glass etching and RCA chemical cleaning, dry oxidation to passivate both surfaces with SiO_2, TiO_2 anti-reflective coating deposition, screen-printing process to form the silver and aluminum/silver metal grids on front and rear face, respectively, firing of the conductive pastes and edge isolation with laser irradiation.

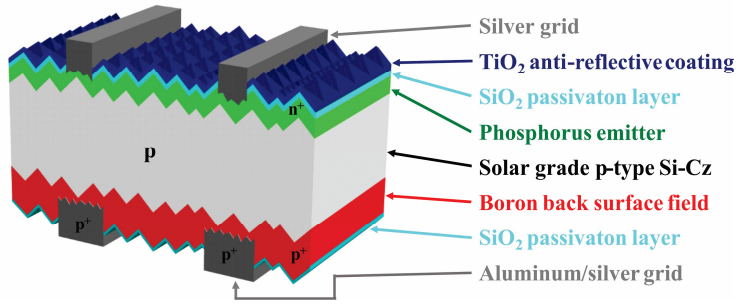

Fig. 1: Configuration of the PERT solar cell developed with boron back surface field and TiO_2/SiO_2 double layer on the phosphorus emitter.

The boron BSF was formed by the deposition of the PBF20 boron solution (Filmtronics) using the spin coating technique. This procedure is used to deposit the uniform thin films and consists in to apply a small amount of the

liquid with boron on the center of the wafer, which is spun at high speed. The boron diffusion was carried out in a quartz tube furnace at 970 °C. In the same thermal step of boron diffusion, the silicon dioxide layer to protect the boron-doped region of the phosphorus diffusion was grown, based on the patent BR1020120306069 (Zanesco and Moehlecke, 2012). The phosphorus n^+ emitter with the sheet resistance of (63 ± 4) Ω/ was produced using $POCl_3$. In the boron BSF the sheet resistance was (42 ± 2) Ω/ .

Based on previous studies (Zanesco et al., 2018[a]), the dry oxidation to passivate the surfaces of the solar cells was performed with two processes: 1) temperature of 800 °C during 45 minutes and 2) temperature of 860 °C and time of 30 minutes. The thickness of the SiO_2 layer was higher in the phosphorus emitter than in the boron BSF (Ho and Plummer, 1979). The SiO_2 passivation layer grown at 800 °C, was around 50 nm and 10 nm thick in the phosphorus emitter and boron BSF, respectively. The silicon oxide growth at 860 °C resulted in a slightly thicker SiO_2 films. The thickness of SiO_2 passivation layers were approximately 60 nm in the emitter and 14 nm in and BSF (Zanesco et al., 2018[a]).

After the oxidation process, the TiO_2 AR layer was deposited taking into account the thickness of the SiO_2 passivation layer. Specifically, the thickness of the TiO_2 AR coating deposited by electron-beam technique on the front emitter was experimentally optimized. For this reason, the TiO_2 AR coating was ranged from 5 nm to 60 nm. In addition to the solar cells, samples were also prepared and processed together with the solar cells to characterize the TiO_2/SiO_2 double layer.

Then, the silver metal grid, with two busbars, was screen-printed on the front face. The area covered with silver paste was of around 8 %. On the rear face the aluminum/silver paste was screen-printed and the metal grid with two busbar coated about 14.5 % of the total area. The conductive pastes were fired at 860 °C (Zanesco et al., 2018[b]).

Batches with 3 – 6 silicon solar cells with the area of 61.58 cm^2 were processed. All the solar cells were characterized under standard conditions (100 mW/cm^2, AM1.5G and 25°C) in a solar simulator and the average electrical parameters were calculated. The reflectance was measured in five regions of samples prepared in the same process of the solar cells with a spectrophotometer with integrating sphere. The thickness of the TiO_2 and TiO_2/SiO_2 layer was measured with an ellipsometer. The internal quantum efficiency of the solar cells with the highest efficiency, manufactured in each process, was obtained by the measurement of the spectral response and reflectance. Then, the thickness of the layer was optimized comparing the electrical characteristics and the weighted average reflectance (Zhao and Green, 1991) taking into account the spectral response of the solar cell. The TiO_2/SiO_2 double layer was analyzed by the thickness, weighted average reflectance and reflectance before and after the firing process of the conductive pastes in the belt furnace and by the internal quantum efficiency of the solar cells.

3. Results and discussion

3.1. Anti-reflective coating optimization

3.1.1 SiO_2 passivation layer grown at 800 °C

The Tab. 1 presents the average values of the open circuit voltage (V_{oc}), short-circuit current density (J_{sc}), fill factor (FF) and efficiency (η) of the PERT solar cells with the SiO_2 layer grown in dry oxidation at 800 °C during 45 minutes as a function of the thickness of the TiO_2 AR coating (d_{TiO2}). In Tab. 1 and Tab. 2, d_{TiO2} represents the value of the AR coating before the process to fire the silver and aluminum/silver pastes. The AR coating affects mainly the J_{SC}. Then, considering this effect, the selected values of d_{TiO2} were in the range from 33 nm to 42 nm. The average efficiency of 16.3 % was achieved with d_{TiO2} = 42 nm. The fill factor tends to decrease with the increasing of the TiO_2 thickness and reduces the efficiency.

In Tab. 2, the PERC solar cells with the highest efficiency of each process are compared. The J_{SC} of 36.0 mA/cm^2 was obtained with d_{TiO2} = 42 nm, and the efficiency of 16.8 % was achieved with this TiO_2 thickness. The results presented in Tab. 2 confirms that fill factor and also open circuit voltage tend to decrease with the increasing of d_{TiO2}. Then, the d_{TiO2} that leads to the higher short-circuit current density and efficiency was 42 nm.

Tab. 1: Average open circuit voltage (V_{oc}), short-circuit current density (J_{sc}), fill factor (FF) and efficiency (η) of the PERT silicon solar cells with the SiO_2 passivation layer grown in dry oxidation at 800 °C as a function of the thickness of the TiO_2 AR coating (d_{TiO2}). d_{TiO2} represents the value of the AR coating before the process to fire the silver and aluminum/silver pastes in the belt furnace.

Process	Number of cells	d_{TiO2} (nm)	V_{oc} (mV)	J_{sc} (mA/cm^2)	FF	η (%)
PO800-10	03	13	606.3 ± 0.8	33.7 ± 0.3	0.785 ± 0.002	16.1 ± 0.2
PO800-15	04	21	604.9 ± 0.3	33.5 ± 0.1	0.783 ± 0.002	15.9 ± 0.1
PO800-20	05	33	596 ± 3	35.2 ± 0.3	0.770 ± 0.007	16.1 ± 0.2
PO800-25	03	42	597 ± 2	35.0 ± 1.5	0.779 ± 0.002	16.3 ± 0.7
PO800-30	03	52	601 ± 2	34.9 ± 0.8	0.759 ± 0.011	15.9 ± 0.5
PO800-35	03	60	601 ± 4	34.9 ± 0.7	0.768 ± 0.012	16.1 ± 0.3

Tab. 2: Electrical characteristics of the silicon solar cells with the highest efficiency achieved in each process as a function of the thickness of the TiO_2 AR coating (d_{TiO2}) and passivated with SiO_2 grown at 800 °C.

Process	d_{TiO2} (nm)	V_{oc} (mV)	J_{sc} (mA/cm^2)	FF	η (%)
PO800-10	13	607.1	34.1	0.786	16.3
PO800-15	21	605.3	33.6	0.784	15.9
PO800-20	33	597.4	35.6	0.775	16.5
PO800-25	42	598.6	36.0	0.777	16.8
PO800-30	52	598.8	35.9	0.771	16.6
PO800-35	60	596.7	35.7	0.766	16.3

3.1.2 SiO_2 passivation layer grown at 860 °C

The Tab. 3 shows the average electrical parameters of the solar cells with the SiO_2 layer grown with dry oxidation at 860 °C during 30 minutes and Tab. 4 summarizes the results of the solar cells with the highest efficiency as a function of d_{TiO2} (before the firing process). The average efficiency of 15.7 % was lower than that obtained in solar cells with oxidation process at 800 °C.

Taking into account the short-circuit current density, the optimized d_{TiO2} can be in the range from 15 nm to 48 nm. The higher efficiencies were obtained with d_{TiO2} around 13 - 15 nm because the fill factor and open circuit voltage were slightly affected by the increasing of the TiO_2 thickness. This behavior was also observed in the solar cells processed at 800 °C. Then, the d_{TiO2} that resulted in the higher efficiencies was around 13 – 15 nm.

Tab. 3: Average electrical characteristics of the silicon solar cells with the SiO_2 passivation layer grown in dry oxidation at 860 °C as a function of the thickness of the TiO_2 AR coating (d_{TiO2}). d_{TiO2} represents the value of the AR coating before the process to fire the silver and aluminum/silver pastes in the belt furnace.

Process	Number of cells	d_{TiO2} (nm)	V_{oc} (mV)	J_{sc} (mA/cm^2)	FF	η (%)
PO860-05	03	4	596 ± 2	33.3 ± 0.1	0.775 ± 0.003	15.4
PO860-10	03	13	599 ± 3	33.5 ± 0.1	0.783 ± 0.002	15.7 ± 0.1
PO860-15	06	15	592 ± 4	33.7 ± 0.4	0.778 ± 0.003	15.5 ± 0.3
PO860-20	06	22	578 ± 14	33.8 ± 0.4	0.772 ± 0.003	15.1 ± 0.6
PO860-30	03	48	572 ± 6	33.7 ± 0.2	0.773 ± 0.002	14.9 ± 0.2

Tab. 4: Electrical characteristics of the silicon solar cells with the highest efficiency as a function of the thickness of the TiO_2 AR coating (d_{TiO2}) and passivated with SiO_2 grown at 860 °C.

Process	d_{TiO2} (nm)	V_{oc} (mV)	J_{sc} (mA/cm^2)	FF	η (%)
PO860-5	4	597.4	33.2	0.777	15.4
PO860-10	13	601.1	33.5	0.785	15.8
PO860-15	15	596.4	34.0	0.780	15.8
PO860-20	22	592.9	34.3	0.775	15.8
PO860-30	48	575.2	33.9	0.771	15.0

3.2. Evaluation of the TiO_2 and TiO_2/SiO_2 layer

The Tab. 5 and Tab. 6 show the thickness of the TiO_2 AR coating, thickness of the TiO_2/SiO_2 double layer ($d_{TiO2-SiO2}$) and weighted average reflectance (ρ_W) of the TiO_2/SiO_2 stack, before and after the firing of the conductive

pastes. In Tab. 5, the results are compared for solar cells with SiO_2 passivation layer processed at 800 °C. After the firing process, the thickness of the TiO_2 layer and TiO_2/SiO_2 stack diminished. The reduction of the TiO_2/SiO_2 double layer ranged from 3 nm to 7 nm and was caused by the reduction of the TiO_2 layer. After the firing process, the lowest weighted average reflectance of 2.8 % occurred in the range of d_{TiO2} from 37 nm to 45 nm and was similar to the value obtained before the thermal process. Taking into account the efficiency presented in Tab. 1, the value of d_{TiO2}, that decreased from 42 nm to 37 nm with the firing process, lead to higher efficiency and lower reflectance. The thickness of the double layer was of 89 nm, after the firing of the conductive pastes.

When the SiO_2 layer was thermally grown at 860 °C, the weighted average reflectance after the firing of the conductive pastes was the same, but ρ_W = 2.8 % was found in the range of d_{TiO2} from 18 nm to 43 nm, as Tab. 6 summarizes. In this case, the reduction of the TiO_2/SiO_2 layer with firing process was similar to the results presented in Tab. 5, if the value obtained for d_{TiO2} = 14 nm is not taking into account. Comparing the electrical parameters showed in Tab. 3 and the ρ_W in Tab. 6, we can notice that low weighted average reflectance corresponds to the high short-circuit current density. On the other hand, the greater efficiencies were obtained for d_{TiO2} of 11 - 14 nm, due to the trends of the decreasing of the fill factor and open circuit voltage with the increasing of the AR layer. Then, the selected thickness of the TiO_2 layer was 14 nm (after firing process), that results in the double layer of 71 nm, taking into account the higher J_{SC} and efficiency.

Tab. 5: Thickness of the TiO_2 AR coating (d_{TiO2}), thickness of the TiO_2/SiO_2 double layer ($d_{TiO2\text{-}SiO2}$) and weighted average reflectance (ρ_W) of the TiO_2/SiO_2 stack before and after the firing of the Ag and Al/Ag pastes and reduction of the TiO_2/SiO_2 thickness ($\Delta d_{TiO2\text{-}SiO2}$) after the firing process. The SiO_2 passivation layer was grown at 800 °C.

Process	Before firing process			After firing process			Reduction
	d_{TiO2} (nm)	$d_{TiO2\text{-}SiO2}$ (nm)	ρ_W (%)	d_{TiO2} (nm)	$d_{TiO2\text{-}SiO2}$ (nm)	ρ_W (%)	$\Delta d_{TiO2\text{-}SiO2}$ (nm)
PO800-10	13	65	3.7	10	62	3.8	3
PO800-15	21	73	3.0	15	67	3.3	6
PO800-20	33	85	2.7	28	80	2.9	5
PO800-25	42	94	2.8	37	89	2.8	5
PO800-30	52	103	2.9	45	97	2.8	6
PO800-35	60	112	3.4	53	105	3.0	7

Tab. 6: Thickness of the TiO_2 AR coating (d_{TiO2}), thickness of the TiO_2/SiO_2 double layer ($d_{TiO2\text{-}SiO2}$) and weighted average reflectance (ρ_W) of the TiO_2/SiO_2 stack before and after the firing of the Ag and Al/Ag pastes and reduction of the TiO_2 (Δd_{TiO2}) and TiO_2/SiO_2 ($\Delta d_{TiO2\text{-}SiO2}$) thickness after the firing process. The SiO_2 passivation layer was grown at 860 °C.

Process	Before firing process			After firing process			Reduction
	d_{TiO2} (nm)	$d_{TiO2\text{-}SiO2}$ (nm)	ρ_W (%)	d_{TiO2} (nm)	$d_{TiO2\text{-}SiO2}$ (nm)	ρ_W (%)	$\Delta d_{TiO2\text{-}SiO2}$ (nm)
PO860-5	4	61	4.3	3	58	4.5	3
PO860-10	13	70	3.1	11	66	3.5	4
PO860-15	15	72	3.1	14	71	3.3	1
PO860-20	22	82	2.6	18	75	2.8	7
PO860-30	48	105	3.0	43	100	2.8	5

The reflectance of the TiO_2/SiO_2 layer measured in five regions of the sample without metal grid and with SiO_2 grown at 800 °C and TiO_2 thickness of 37 nm (after the firing process) is compared in Fig. 2 with the reflectance of sample processed at 860 °C and TiO_2 thickness of 14 nm. The reflectance was measured after the firing of the conductive pastes. The uniformity of the AR layer is higher in Fig. 2-a, when the SiO_2 was grown at 800 °C, than in Fig. 2-b. The oxidation at temperature of 860 °C produced a SiO_2 layer with more variation of the thickness in the same silicon wafer than the other oxidation process. The Fig. 2-a indicates that the minimum reflectance of around 0.8 % occurred in the range of wavelength from 580 to 630 nm. Meanwhile, in samples with silicon oxide grown at 860 °C, the minimum reflectance occurred in shorter wavelengths. In this case, the minimum reflectance of about 1 % is observed in the range of wavelengths from 500 to 550 nm.

The Fig. 3-a shows the reflectance of the TiO_2/SiO_2 layer measured in the center of the silicon wafer after the

firing process and SiO_2 growth at 800 °C as a function of the thickness of the AR coating and the Fig. 3-b presents the results obtained in samples processed at 860 °C. For the two oxidation temperatures, with the increasing of the TiO_2 thickness, that increased the TiO_2/SiO_2 layer, the minimum reflectance shifted to larger wavelengths, rising the reflectance in shorter wavelengths. The lower reflectances were observed for wavelengths longer than 650 nm and high TiO_2 thickness.

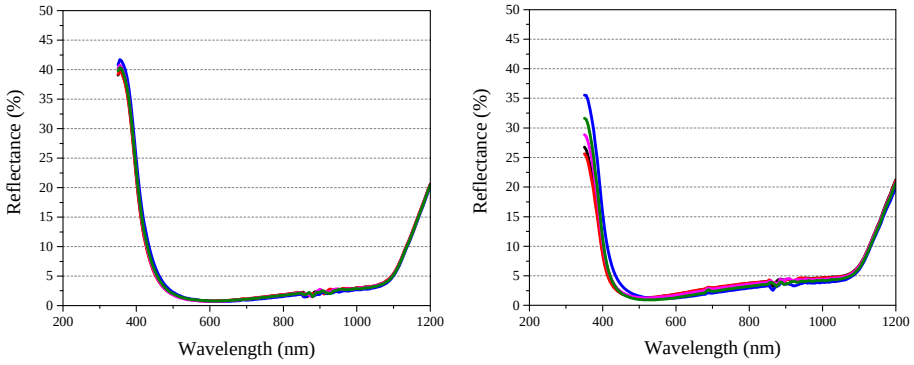

Fig. 2: Reflectance of the TiO_2/SiO_2 layer measured in five regions of the sample without metal grid, after the firing of the conductive pastes, with SiO_2 grown (a) at 800 °C and TiO_2 thickness of 37 nm and (b) at 860 °C and TiO_2 thickness of 14 nm.

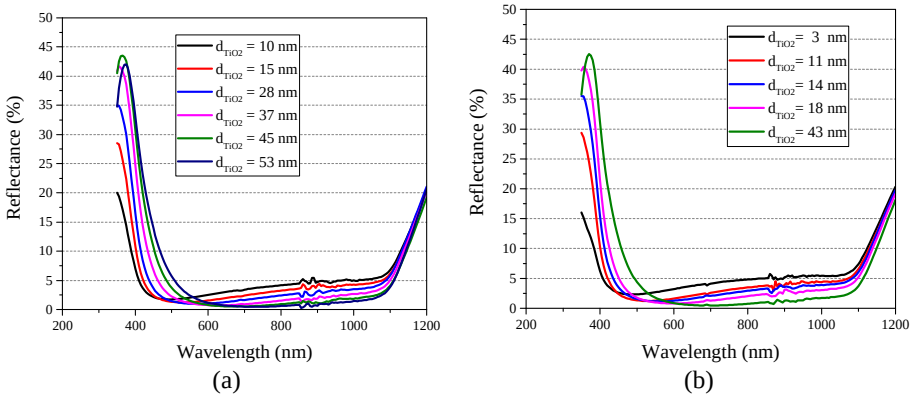

Fig. 3: Reflectance of the TiO_2/SiO_2 layer after the firing of the silver and aluminum/silver pastes with SiO_2 grown (a) at 800 °C and (b) at 860 °C as a function of the thickness of the TiO_2 layer. The reflectance was measured in samples without metal grid.

The influence of the firing process in the SiO_2/TiO_2 double layer is shown in Fig. 4. The behavior of the reflectance changes mainly in wavelengths shorter than 600 nm when the firing of the conductive pastes is performed. Specifically, the reflectance reduced in short wavelengths and this effect is observed mainly for d_{TiO2} greater than 10 nm. This effect is observed in the SiO_2 layer grown at 800 °C and 860 °C, as Fig. 4-a and Fig. 4-b show.

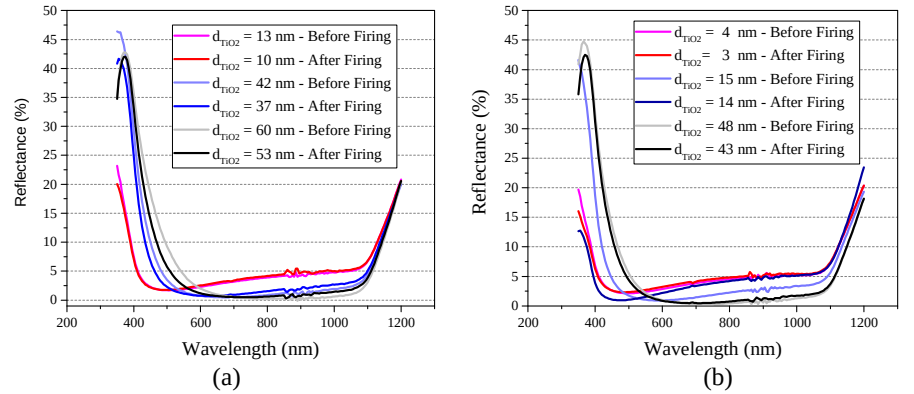

Fig. 4: Reflectance of the TiO_2/SiO_2 layer measured before and after the firing of the conductive pastes with SiO_2 grown (a) at 800 °C and (b) at 860 °C. The reflectance was measured in the sample without metal grid.

3.3. Analysis of the internal quantum efficiency

The Fig. 5 shows the internal quantum efficiency (IQE) of the solar cells with the highest efficiency achieved in each oxidation process as a function of the TiO_2 thickness. The IQE of solar cells with SiO_2 grown at 800 °C is presented in Fig. 5-a and the result of the devices processed at temperature of 860 °C is compared in Fig. 5-b. In both set of solar cells, i. e., with SiO_2 produced by oxidation at 800 °C and 860 °C, the IQE falls down for wavelengths higher than 700 nm with the reduction of the TiO_2 thickness. Specifically, a low IQE is observed in wavelengths higher than 700 nm for the thinner TiO_2 coating. In this range of wavelengths, the internal quantum efficiency increases up to the TiO_2 thickness of 37 nm (Fig 5-a) and 14 nm (Fig 5-b), confirming the selected d_{TiO2}. In the solar cells passivated with SiO_2 grown at 800 °C and 860 °C, the TiO_2 AR coating deposited on the front emitter probably causes the internal reflection of irradiance in the front face for wavelengths higher than 700 nm and this phenomenon is enhanced for $d_{TiO2} \geq$ of 37 nm and 14 nm, respectively. The higher open circuit voltages measured in the solar cells with lower TiO_2 thicknesses may be explained due to the reduction of the minority charge carrier recombination in the rear region because the depletion of the minority carriers.

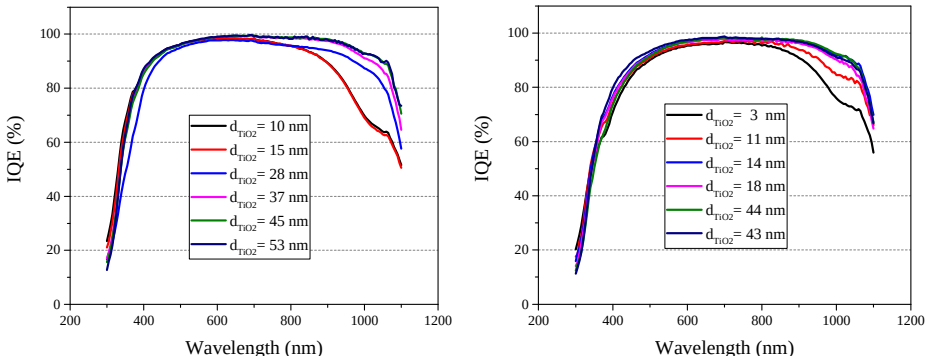

(a) (b)

Fig. 5: Internal quantum efficiency of solar cells with the highest efficiency achieved in each batch as a function of the TiO_2 thickness with SiO_2 grown in the oxidation performed at (a) 800 °C and (b) 860 °C.

4. Conclusions

In this paper, the influence of the TiO_2 anti-reflective coating deposited over the SiO_2 passivation layer grown at 800 ºC and 860 ºC on the front emitter of PERT solar cells was analyzed. The higher values of the short-circuit current density were found with TiO_2 thickness from 33 nm to 42 nm and from 15 nm to 48 nm in solar cells processed at 800 ºC and at 860 °C, respectively. The fill factor and open circuit voltage tend to decrease with the increasing of the TiO_2 thickness. Consequently, the average efficiency of 16.3 % was obtained with d_{TiO2} = 42 nm and solar cells processed at 800 °C. This efficiency was higher than the value of 15.7 % achieved in solar cells with oxidation at 860 °C and d_{TiO2} around 13 - 15 nm.

The firing of the silver and aluminum/silver pastes diminished the TiO_2/SiO_2 double layer thickness, due to the phase transformation of the TiO_2 and the reduction ranged from 3 nm to 7 nm. After the firing process, the lowest weighted average reflectance of 2.8 % occurred in the range of d_{TiO2} from 37 nm to 45 nm and from 18 nm to 43 nm, for samples processed at 800 ºC and 860 ºC, respectively. Taking into account the efficiency and the weighted average reflectance, the selected thickness of the TiO_2 layer was 37 nm and 14 nm (after firing process), resulting in the double layer of 89 nm and 71 nm, for solar cells with oxidation at 800 ºC and 860 ºC.

The uniformity of the TiO_2/SiO_2 double layer was higher when the SiO_2 was grown at 800 °C. For this temperature, the minimum reflectance of around 0.8 % occurred in the range of wavelengths from 580 to 630 nm. With the oxidation process at 860 °C, the minimum reflectance of around 1 % occurred in shorter wavelengths from 500 to 550 nm.

The firing of the conductive pastes caused the reduction of the reflectance in short wavelengths and this effect was observed mainly for d_{TiO2} greater than 10 nm. The solar cells with thinner TiO_2 coatings shown a low internal quantum efficiency in wavelengths higher than 700 nm. In this range of wavelengths, the internal

quantum efficiency increased up to the TiO_2 thickness of 37 nm (800 ºC) and 14 nm (860 ºC), confirming the selected TiO_2 thicknesses.

5. Acknowledgments

The authors gratefully acknowledge the financial support of the "Eletrosul Centrais Elétricas S.A.", contract 1110140010, the National Council for Scientific and Technological Development (CNPq) and the Coordination for the Improvement of Higher Education Personnel (CAPES).

6. References

Ali, K., Khan S. A., Jafri, M. Z. M., 2014. Effect of double layer (SiO_2/TiO_2) anti-reflective coating on silicon solar cells. International Journal of Electrochemical Science. 9, 7865 – 7874.

Chen, Y.; Zhong, S.; Tan, M.; Shen, W., 2017. SiO_2 passivation layer grown by liquid phase deposition for silicon solar cell application. Energy. 11, 52-59.

Colville F 2017 PERC solar cell production to exceed 15 GW in 2017 [www.pv-tech.org/editors-blog/perc-solar-cell-production-to-exceed-15gw-in-2017].

Green, M. A., 2015. The passivated emitter and rear cell (PERC): From conception to mass production Solar. Energy Materials &Solar Cells. 143, 190-197.

Ho, C.P.; Plummer, J.D., 1979. Si/SiO_2 interface oxidation kinetics: A physical model for the influence of high substrate doping levels, Journal of the Electrochemical Society. 126 (9), 1523-1530.

ITRPV, 2019. Results 2019 International technology roadmap for photovoltaic 10th edition [www.itrpv.vdma.org].

Kanda, H.; Uzum, A.; Harano, N.; Yoshinaga, S.; Ishikawa, Y.; Uraoka, Y.; Fukui, H.; Harada, T.; Ito, S., 2016. Al_2O_3/TiO_2 double layer anti-reflection coating film for crystalline silicon solar cells formed by spray pyrolysis, Energy Science and Engineering. 4(4), 269–276.

Lee, Y., Ho, W-J., Yeh, W., 2015. Fabrication of silicon solar cell with >18% efficiency using spin-on-film processing for phosphorus diffusion and SiO_2 graded index TiO_2 anti-reflective coating. Applied Surface Science. 354, 20-24.

Lelièvre, J. F.; Kafle, B.; Saint-Cast, P.; Brunet, P.; Magnan, R.; Hernandez, E.; Pouliquen, S.; Massines, F., 2019. Efficient silicon nitride SiNx:H antireflective and passivation layers deposited by atmospheric pressure PECVD for silicon solar cells. Progress in Photovoltaics: Research and Applications, EU PVSEC PAPER, p. 1-13. [DOI: 10.1002/pip.3141].

Liu, J.; Yao, Y.; Xiao, S.; Gu, G., 2018 Review of status developments of high-efficiency crystalline silicon solar cells. Journal of Physics D: Applied Physics. 51, 1-12.

Glunz, S. W.; Feldmann F., 2018. Cells SiO_2 surface passivation layers – a key technology for silicon solar cells. Solar Energy Materials and Solar Cells. 185, 260-269.

Huang, H,; Modanese, C.; Sun, S.; Gastrow, G. V., Wang, J.; Pasanen, T. P.; Li, S., 2018. Effective passivation of p^+ and n^+ emitters using $SiO_2/Al_2O_3/SiN_x$ stacks: Surface passivation mechanisms and application to industrial p-PERT bifacial Si solar cells. Solar Energy Materials and Solar Cells. 186, 356-364.

Preissler, N.; Amkreutz, D,; Dulanto, J.; Töfflinger, J. A. Trinh, C., 2018. T. Passivation of Liquid-Phase Crystallized Silicon With PECVD-SiNx and PECVD-SiNx/SiOx. Physica Status Solidi A. 215, 1-9. [DOI: 10.1002/pssa.201800239].

Rahman, M. Z. and Khan, S. I., 2012. Advances in surface passivation of c-Si solar cells. Materials for Renewable and Sustainable Energy 1 1-11. [DOI: 10.1007/s40243-012-0001].

Sali, S.; Kermadi, S.; Zougar, .L.; Benzaoui, B.; Saoula, N.; Mahdid, K.; Aitameur, F.; Boumaour, M., 2017. Nanocrystalline proprieties of TiO_2 thin film deposited by ultrasonic spray pulverization as an anti-reflection coating for solar cell applications. Journal of Electrical Engineering. 68 (7), 24-30.

Suh, D., 2019. Thermal stability of Al_2O_3/TiO_2 stacks for boron emitter passivation on ntype silicon solar cells. Thin Solid Films. 669, 60 – 64.

Zanesco, I.; Moehlecke, A., 2012. Impurity diffusion process in silicon wafers to fabricate solar cells (Process of diffusion of dopants in silicon wafers to manufacture solar cells) Brazilian patent PI12030606, BR 10 2012 030606 9.

Zanesco, I.; Moehlecke, Adriano., 2015. Analysis of the Silicon Dioxide Passivation and Forming Gas Annealing in Silicon Solar Cells. In: ISES Solar World Congress 2015, 2016, Daegu. Proceedings of the ISES Solar World Congress 2015, pp. 1-9.

Zanesco, I.; Razera, R. A. Z. ; Moehlecke, A., 2018[a]. Analysis of the SiO_2 passivation of the rear and front surface of solar cells with selective back surface field. Materia-Rio de Janeiro, 22, 11924-9. In Portuguese.

Zanesco, I.; Crestani, T. ; Moehlecke, A. ; Aquino, J. ; Razera, R. A. Z. ; Model, J. C. M. ; Ly, M. ; Gonçalves, V. A., 2018[b]. Development of the solar cell with higher efficiency in Brazil with industrial process. Anais do VII Congresso Brasileiro de Energia Solar. São Paulo, SP, pp. 1-9. In Portuguese.

Zhao J, Green M., 1991. Optimized antireflection coatings for high-efficiency silicon solar cells. IEEE Transactions on Electron Devices. 38(8), 1925-1934.